3D PHONONIC CRYSTALS

Ultrasonic Wave Transport and Spectroscopy in Complex Media II

J. H. PAGE[1], SUXIA YANG[2] AND M. L. COWAN[3]
Department of Physics and Astronomy, University of Manitoba, Winnipeg MB R3T 2N2 Canada

ZHENGYOU LIU
Department of Physics, Wuhan University, Wuhan 430072 China

AND

C. T. CHAN AND PING SHENG
Department of Physics, Hong Kong University of Science and Technology, Clear Water Bay, Kowloon, Hong Kong

Abstract. Recent progress in the use of ultrasonic experiments and Multiple Scattering Theory to investigate wave transport in three-dimensional phononic crystals is summarized. Through appropriate choice of material properties, complete band gaps can be realized for acoustic or elastic waves in such structures. This has allowed us to demonstrate the tunnelling of ultrasound through the band gap and to explore the unexpected effect of absorption on evanescent waves in crystals. Wave propagation above the gap has also been investigated, where we have shown that anisotropy of the wave speeds leads to the focussing of ultrasound without the curved surfaces usually employed in lenses. These ultrasonic experiments and their interpretation using Multiple Scattering Theory illustrate the important contribution that the study of phononic crystals can make to learning about wave scattering and transport in ordered mesoscopic materials.

1. Introduction

Phononic crystals are periodic composite materials with variations of velocity and density on length scales comparable with the wavelength of sound (or ultrasound) [4, 5, 6, 7, 8, 9, 10, 11, 12, 13, 14, 15, 16, 17]. Because the scattering contrast between the component materials depends on dif-

ferences in both density and phase velocity, phononic crystals with very strong scattering can be realized experimentally, making such materials interesting candidates for studying the profound effects of lattice structure on wave propagation. This is one of the main reasons for the considerable growth of interest in phononic crystals that has occurred during the last decade. Much of this interest has focussed on phononic bandgaps, which correspond to ranges of frequency in which acoustic or elastic waves cannot propagate due to Bragg scattering, and are analogous to photonic band gaps [18, 19, 20] for electromagnetic waves. Through appropriate choice of materials, it has been demonstrated by a combination of theory and experiment that complete band gaps can be readily achieved for acoustic and elastic systems, so that wave propagation is forbidden in all directions. This is in sharp contrast with photonic materials, where engineering complete spectral gaps in three dimensions has been a difficult experimental challenge.

In this paper we describe a combination of experimental and theoretical results on ultrasonic wave transport in three-dimensional (3D) phononic cystals [13, 14, 15, 16, 17], which have been less studied experimentally than 2D structures [7, 8, 9, 10, 16], possibly because 3D structures have been considered more difficult to fabricate. After a brief description of the crystals used in our experiments and the expected band structures, we summarize recent pulse propagation experiments in which both amplitude and phase information is measured, allowing the transmission coefficient, the dispersion relation and the wave propagation dynamics to be investigated. These experiments are compared with the predictions of Multiple Scattering Theory (MST), which is ideally suited to the spherical scattering geometry of our crystals. This combination of experiment and theory is used to investigate two quite different types of wave phenomena that result from the underlying crystal structure: ultrasound tunnelling through the band gap and the focussing of ultrasound without the usual curved surfaces employed in traditional lenses. Some results of near field imaging experiments are also reported.

2. Our 3D Phononic Crystals and their Band Structures

The crystals used in our experiments consist of close-packed periodic arrays of spherical beads surrounded by a liquid or solid matrix. Both hcp and fcc arrays were assembled by placing the beads carefully by hand in a hexagonal template that was precisely machined to force the beads into triangular layers. The layers were stacked vertically in either an ABAB.. or ABCABC... sequence to form slabs with a hexagonal (c-axis $\perp$ layers) or face-centred cubic ([111]-axis $\perp$ layers) structure, respectively. For the fcc

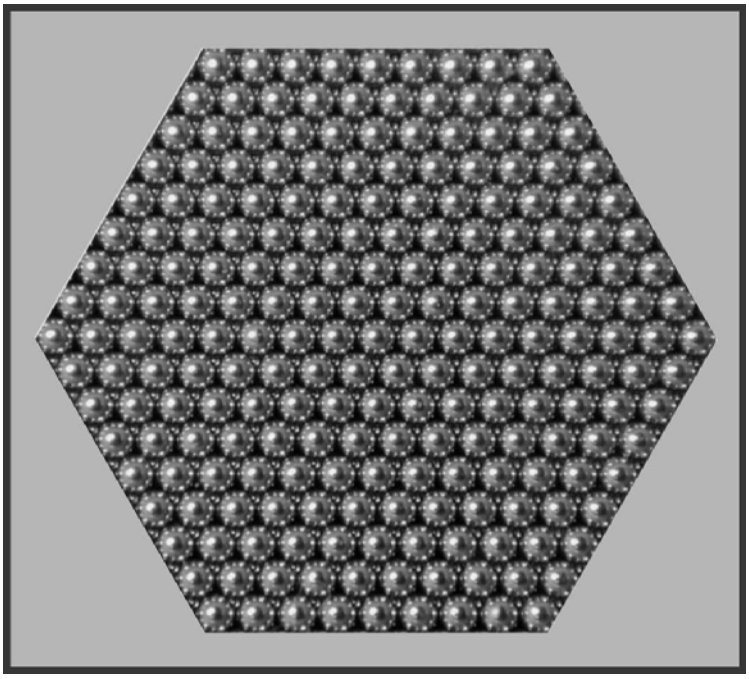

Figure 1. Picture of the top surface of a hcp phononic crystal consisting of monodisperse 0.8-mm-diameter stainless steel beads in water.

structures, the template was designed with sloping sides to ensure that the layers were arranged in the correct sequence [21]. The beads were made of either stainless steel or tungsten carbide, and the matrix was either water or epoxy. For all these crystals, the scattering contrast was very high (the acoustic impedance ratios of bead to matrix ranged from 30 to 60) and the beads were very monodisperse (e.g. for the tungsten carbide beads, the sphere diameter d was 0.8000 ± 0.0006 mm), so that very high quality crystals could be prepared with patience and good manual dexterity. An example of one of the crystals is shown in Fig. 1, illustrating the excellent regularity of the structure that was achieved.

Ultrasonic pulse propagation through the crystals was measured by placing the crystals in a large water tank in between two immersion transducers, which acted as generator and detector [15, 17]. For the water-matrix crystals, it was necessary to keep the crystals in the template during the measurements, so that the pulses also propagated through the bottom plate of the holder; to avoid complications in the analysis of the data, the thickness of the substrate was chosen to be sufficiently large that ultrasonic reflections in the substrate could be separated temporally and removed

from the subsequent analysis of the signal transmitted through the crystal. The frequency dependence of the phase velocity, the group velocity and the transmission coefficient was then measured by comparing the transmitted pulses with reference pulses that had travelled once through the substrate alone.

Before considering the experimental results, it is instructive to consider the theoretical band structures for three of the eight possible combinations of materials. These band structure calculations were performed using the MST [10] and are shown in Fig. 2. For a hcp crystal of steel beads in water (Fig. 2(a)), there is a reasonably large stop band along the c-axis, but the gap almost closes between the M and K points, so there is only a tiny complete gap in this material. Increasing the density contrast, and changing the symmetry from hcp to fcc, results in a much larger complete gap, as shown by the calculations for fcc tungsten carbide beads in water in Fig. 2(b) [22]. In this case, the width of the complete gap, $\Delta\omega/\omega_{\text{centre}}$ is 19%. Figure 2(c) shows the effect of replacing the liquid water matrix with solid epoxy. This changes the scattering, as the matrix can support both longitudinal and transverse polarizations, and results in an even bigger compete gap, with $\Delta\omega/\omega_{\text{centre}} = 90\%$, even though the longitudinal impedance contrast is reduced. However, the epoxy is quite lossy, and the absorption in the crystal becomes significant, so we will focus instead on the second system, fcc tungsten carbide beads in water, in the remainder of this paper.

To compare the theory more directly with the results of our pulsed transmission experiments, we use a layer MST to calculate the transmitted field though crystals consisting of a finite number of layers [13]. For a sample of thickness L, the transmitted field as a function of frequency ω can be written as

$$T(L,\omega) = A(L,\omega)\exp[i\phi(L,\omega)], \tag{1}$$

where A and ϕ are the amplitude and cumulative phase relative to the input field. Thus, the amplitude transmission coefficient is simply $|T(L,\omega)| = A(L,\omega)$, and the phase and group velocities, v_p and v_g, can be determined from cumulative phase in the usual way:

$$v_p(\omega) = \frac{\omega}{k} = L\frac{\omega}{\phi} = \frac{L}{t_p} \tag{2}$$

$$v_g(\omega) = \frac{d\omega}{dk} = L\frac{d\omega}{d\phi} = \frac{L}{t_g} \tag{3}$$

Here k is the wave vector, and t_p and t_g are the phase delay and group delay times. This layer MST is expected to give an accurate description of our experimental results, as it corresponds closely to the experimental geometry for measurements through slab-shaped samples.

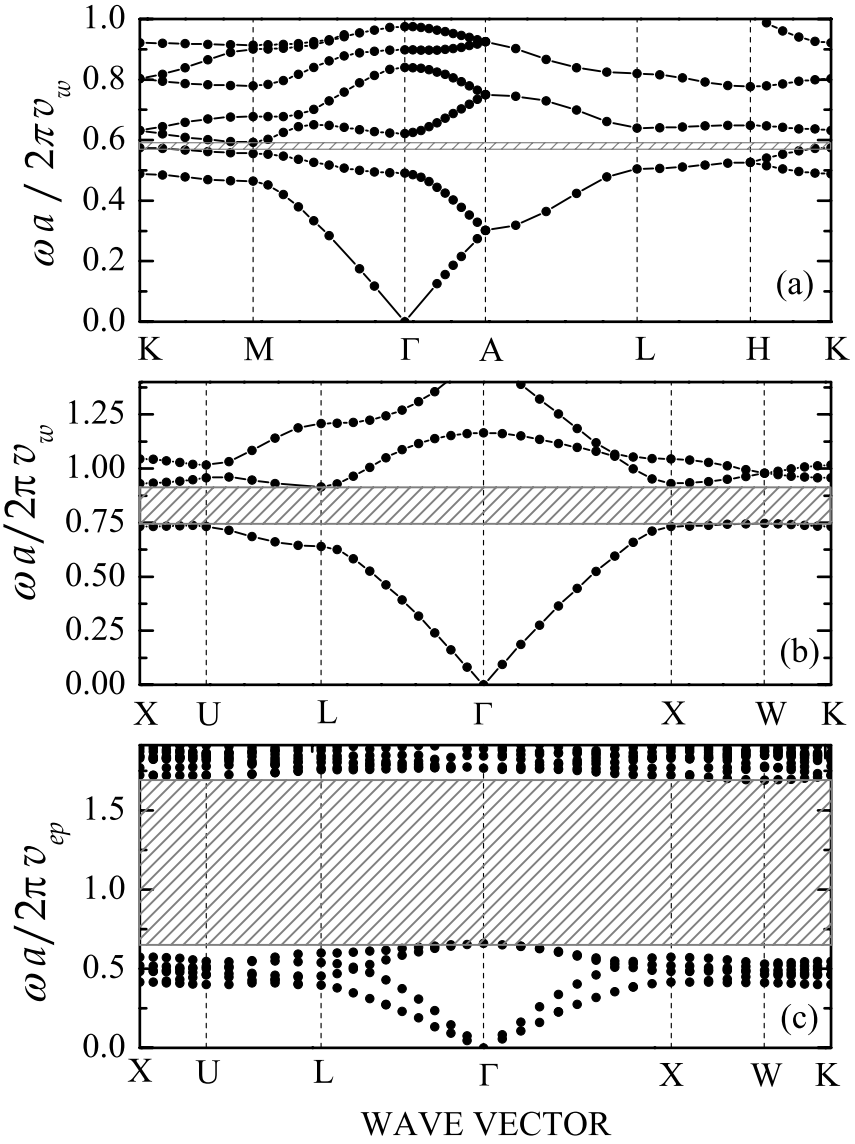

Figure 2. Band structure calculated using the Multiple Scattering Theory for (a) a hcp phononic crystal of stainless steel beads immersed in water, (b) a fcc phononic crystal of tungsten carbide beads in water, and (c) a fcc phononic crystal of tungsten carbide beads in epoxy. Here a is the lattice constant, and v_w and v_{ep} are the (longitudinal) sound velocities in water and epoxy, respectively. The shaded regions indicate the locations of the bandgaps in these materials. The letters denote the high symmetry points of the Brillouin zone.

3. Ultrasound Tunnelling through a Complete Band Gap

The band structure calculation in Fig 2(b) shows that the widest part of the gap for the fcc tungsten-carbide-in-water crystals is predicted along the ΓL direction (‖ [111]). Converting the normalized frequencies shown in this figure to laboratory units, we find that the gap extends over the frequency range from 0.8 to 1.2 MHz. To investigate the behaviour along this direction in the vicinity of the predicted gap, we have measured the frequency dependence of the transmitted signal for a range of sample thicknesses. We used a short pulse centred at 1 MHz, and determined the transmission coefficient from the ratio of the fast Fourier transforms (FFTs) of the transmitted to incident pulses, taking advantage of the excellent linearity of the detection electronics in our experiments. Typical results of these experiments are shown by the symbols in Fig. 3, where they are compared with the predictions of the layer MST. A large dip in the transmission is seen in the expected frequency range, with the dip becoming deeper as the sample thickness increases - a clear signature of a band gap. The smaller oscillations either side of the gap, where the transmission is large, are due to standing wave resonances from boundary reflections at each side of the slab. Overall, the agreement between experiment and theory is good, especially in the gap region. However, the amplitude of the standing wave oscillations is smaller in the experiments than in the theory, a sign of the effects of absorption, which was not included in the theoretical calculation. The fact that the theory and experiments agree well with each other at the frequencies inside the gap suggest that absorption has less effect on the transmission coefficient in this frequency range. Although we only did transmission measurements along one crystal direction, the good agreement between theory and experiments serves as strong evidence for the existence of a wide complete gap, as shown in the theoretically calculated band structure.

One important parameter that characterizes the band gap is the gap width. The band structure calculation only gives the theoretical size and position of a band gap for an infinite sample. Experimentally, samples are finite, and the width and position of the band gap may be thickness dependent. This is borne out by our experiments, which show that the gap width (defined here as the frequency interval between the positions of the peaks in the transmission coefficient at the band edges) decreases as the sample thickness increases, tending towards a constant for our thickest samples (Figure 4). Again, the theory and experiments are in good agreement, especially for the thinner samples.

To look in more detail at the decrease in the transmission as a function of the number of layers in the crystal, we plot the thickness dependence of the

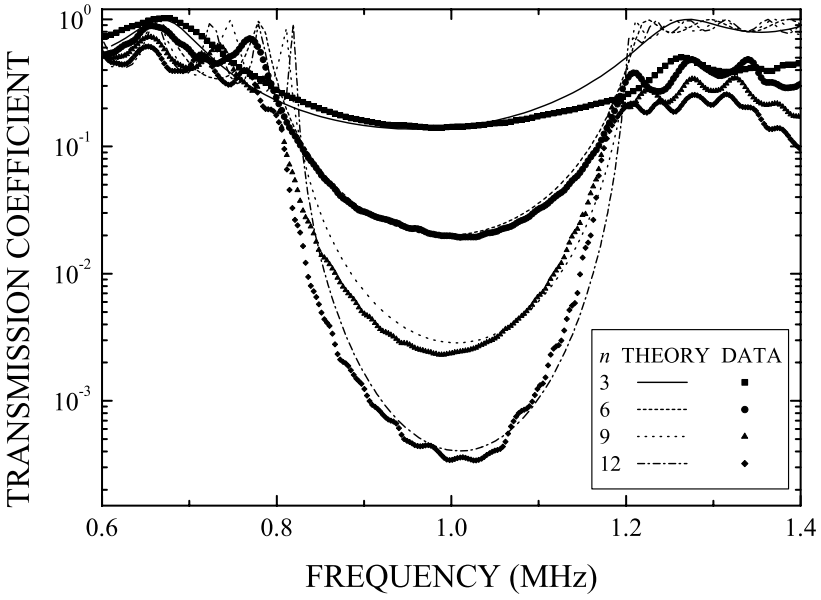

Figure 3. Frequency dependence of the transmission coefficient in the vicinity of the band gap in phononic crystals made from tungsten carbide beads in water. Experimental data for two sample thicknesses (symbols) are compared with the predictions of the layer MST (solid and dashed curves).

transmission coefficient at the gap central frequency of 0.945 MHz in Fig. 5. From this figure, it can be seen that the transmission coefficient decays exponentially as the sample becomes thicker, as expected for evanescent waves in a band gap. From a fit to $T = \exp(-L/(2l))$, we determine the value of the decay length l of the evanescent modes to be 0.54 mm at this frequency, very close to half the lattice constant ($a = \sqrt{2}d = 1.13mm$). The value of l corresponds to an imaginary wave number κ of 0.92 mm^{-1}. This exponential decay with such a small value of the decay length, or large κ, is strongly suggestive that the modes in the gap are evanescent, not propagating, implying that the small signal that does get through thick samples does so by tunnelling. Note that the transmitted intensity for the thickest sample, consisting of only 12 layers, is nearly 7 orders of magnitude smaller than the incident intensity.

The frequency dependence of the cumulative phase ϕ and phase velocity $v_p(\omega) = L\omega/\phi$ in the vicinity of the gap are shown in Fig. 6. Here, data for the 12-layer sample are plotted as solid symbols. The experimental data

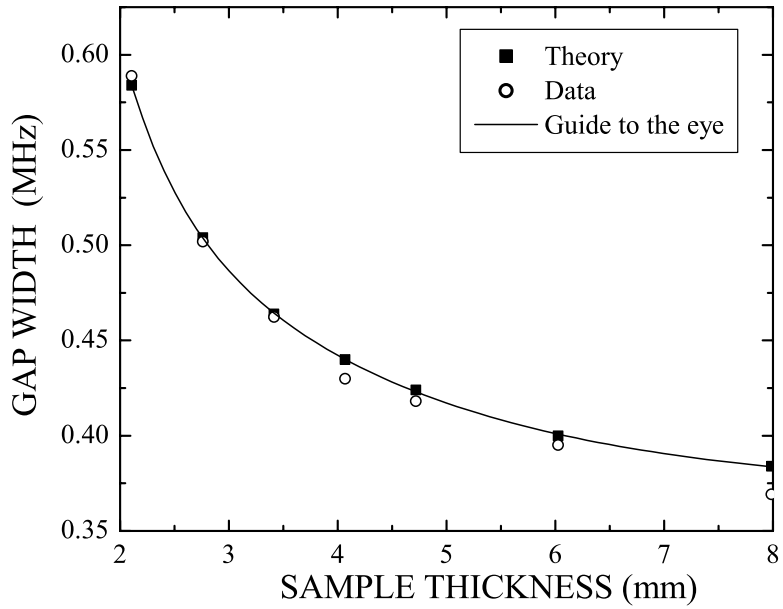

Figure 4. Variation of the gap width with crystal thickness.

for ϕ were obtained from the phase difference of the complex FFTs of the transmitted and input pulses, while resolving any possible ambiguity of 2π in the phase by making use of the condition that the cumulative phase must extrapolate to zero at zero frequency. The cumulative phase increases approximately linearly with frequency at low frequencies, with small oscillations due to the standing wave resonances mentioned above. However, in the gap between 0.8 and 1.2 MHz, there is a plateau in the cumulative phase; in the plateau, there is only a very small linear increase in the phase with frequency, implying a linear increase in the phase velocity and a large group velocity. The behaviour of the phase velocity, shown in Fig. 6(b), confirms this result, and also shows that the phase velocity decreases with frequency on both sides of the gap, reaching values substantially less than the velocity of sound in the matrix material at the highest frequencies shown. The curves show that the behaviour for ϕ and v_p calculated from the transmission MST are in good overall agreement with the experimental data. The phase velocity data can also be used to compute the dispersion curve. Good agreement for the data from the 12-layer crystal is found with the band structure calculation, as shown in [17]. Here we compare

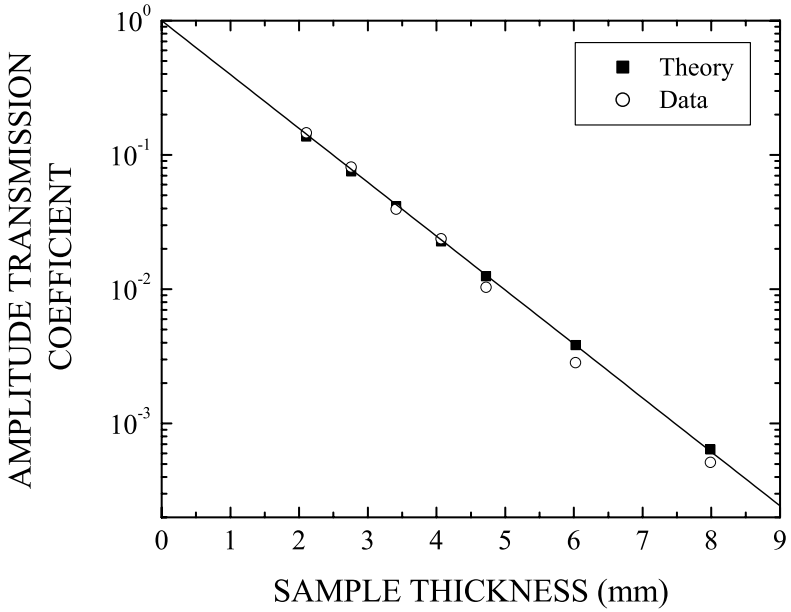

Figure 5. Amplitude transmission coefficient as a function of sample thickness, showing the strong exponential decay. Both the experimental data (solid symbols) and the predictions of the MST (open symbols) are in good agreement with the exponential fit (solid line), which gives a tunnelling decay length of $l = 0.54$ mm.

the experimental dispersion curves in the extended zone scheme (left panel in Fig. 7) with theoretical predictions from the transmission MST theory (right panel in Fig. 7) for three different sample thicknesses. It can be seen that as the sample becomes thicker, the dispersion curve becomes steeper around the boundary of the first Brillouin zone. The overall structure is well captured by the theory, although slight differences can be noticed. The steep slope of the dispersion curve indicates that the group velocity is large in the gap, as the group velocity is equal to the slope of the dispersion curve.

To examine the behaviour of the group velocity in more detail, and to obtain more definitive evidence that tunnelling of ultrasound is occurring in the gap, we have measured the group velocity directly from pulse transmission experiments [17]. These measurements were performed by digitally filtering the input and transmitted pulses using a narrow Gaussian bandwidth, as shown in Fig. 8 for a 12-layer phononic crystal. In this example, the bandwidth was 0.05 MHz and the central frequency was 0.945 MHz,

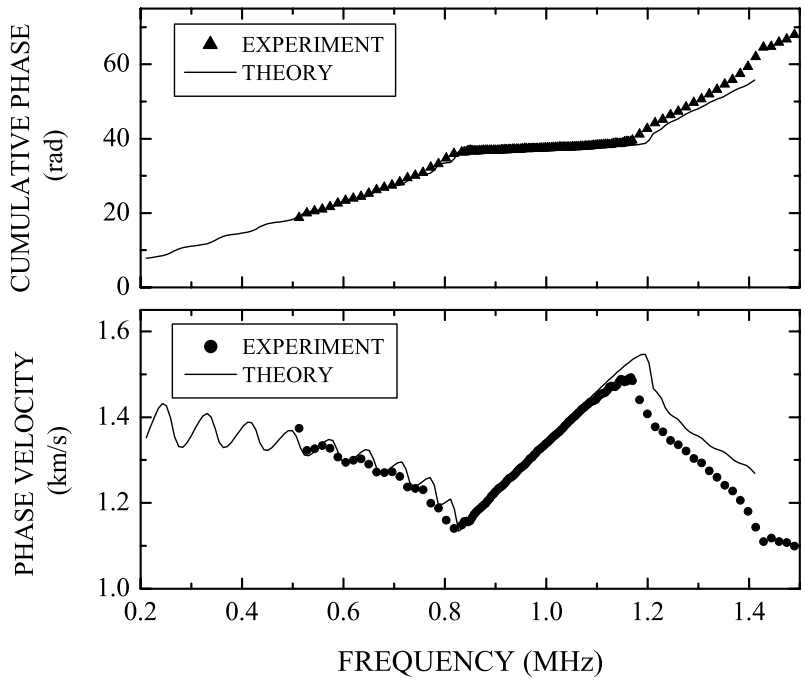

Figure 6. Cumulative phase and phase velocity as a function of frequency for a 12-layer tungsten carbide/water crystal. The solid symbols represent experimental data and the solid curves represent the predictions of the layer MST.

the same frequency in the middle of the gap as in Fig. 5. It is clear from this figure that the pulse travelling through the crystal (bottom panel) arrives very soon after the input pulse (top panel), and travels much more quickly than an identical pulse transmitted through the same thickness of water (middle panel). Note also that the shape of the pulse that has travelled through the crystal is identical with the input pulse, although much reduced in amplitude; this confirms that despite the considerable variation of the phase velocity in the gap region, there is negligible pulse distortion, and the pulse transit time is well defined. The origin of the negligible pulse distortion lies in the linearity of the phase variation with frequency within the gap (see Fig. 6), implying that the group velocity dispersion $dk^2/d^2\omega$ is essentially zero, as we have verified directly in other measurements [21]. The delay between the peak arrival times of the sample and input pulses gives the group delay time t_g, from which we determine the group velocity experimentally ($v_g = L/t_g$).

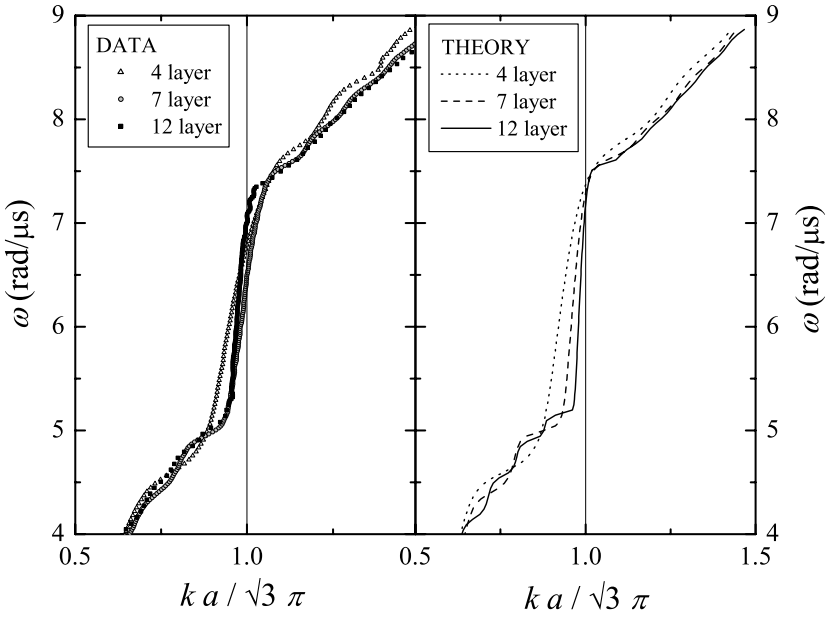

Figure 7. Comparison of the measured dispersion curves along the direction from Γ to L (left panel) with the predictions of the layer MST for the transmission (right panel). The wave vector k is divided by the value at the Brillouin zone boundary for this direction ($\sqrt{3}\pi/a$, where a is the lattice constant). Data and theory for three thickness, corresponding to 4, 7 and 12 layers, are shown.

The frequency dependence of the group delay time in the vicinity of the gap is shown in Fig. 9 for four crystals containing 3, 6, 9 and 12 layers. The behaviour is very striking. Below and above the gap, the group delay time undergoes large oscillations due to the standing wave resonances of the crystal slabs, and the delay time averaged over the oscillations increases in proportion to the sample thickness, as expected. Even the average delay time is quite large at these frequencies, and corresponds to a group velocity less than that of water. By contrast, in the gap, the delay time is very short and *essentially independent of sample thickness,* implying that the group velocity increases linearly with L as the sample becomes thicker. This behaviour shows convincingly that tunnelling is occurring, since one of the remarkable features of tunnelling is that the tunnelling time is independent of thickness [23]. This feature of tunnelling holds quite generally unless the sample or barrier is extremely thin.

To examine the tunnelling behaviour in more detail, we plot the group

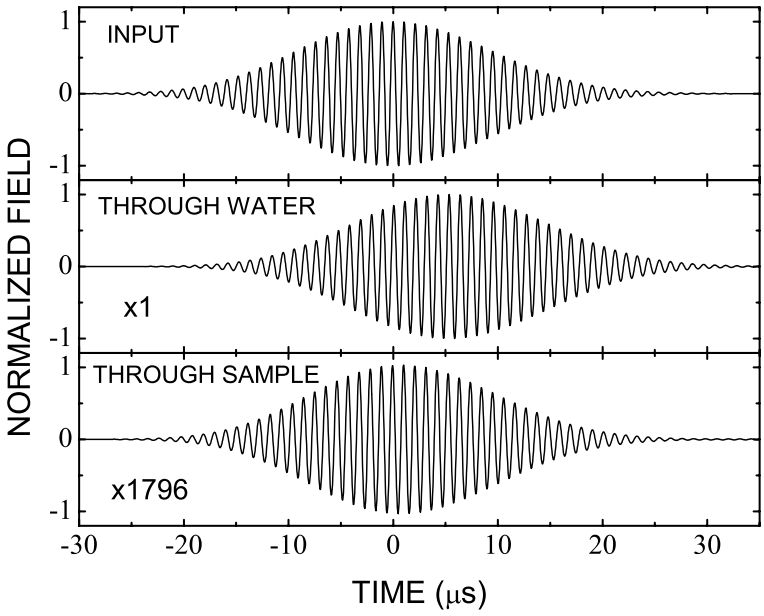

Figure 8. Digitally filtered input and transmitted pulses (top and bottom panels; bandwidth 0.05 MHz) for a 12-layer phononic crystal in the middle of the gap, compared with the pulse transmitted through the same thickness of water (middle panel).

velocity near the centre of the gap at 0.945 MHz as a function of sample thickness L (Fig. 10). This figure shows that the group velocity in the gap increases monotonically with L, both in experiment (triangles) and in MST theory (solid line and squares). Note the large values of the group velocity for thick samples, where experimental and theoretical values can be larger than the longitudinal velocity in both water and tungsten carbide (horizontal dotted lines). However, there is a substantial difference between the theoretical predictions and the experimental results, which we interpret as a consequence of absorption which was not included in the MST calculation [24]. For evanescent waves in the band gap of a phononic crystal, the consequences of absorption are quite interesting. As we have discussed previously [17], the main effect of absorption is to cut off long multiple scattering paths, with the result that the destructive interference of Bragg-scattered waves that give rise to the band gap becomes incomplete. Consequently, in addition to the dominant tunnelling mode, a small propagating component is 'created' by absorption, with an effective wave vector determined by the incomplete cancellation of the Bragg scattered

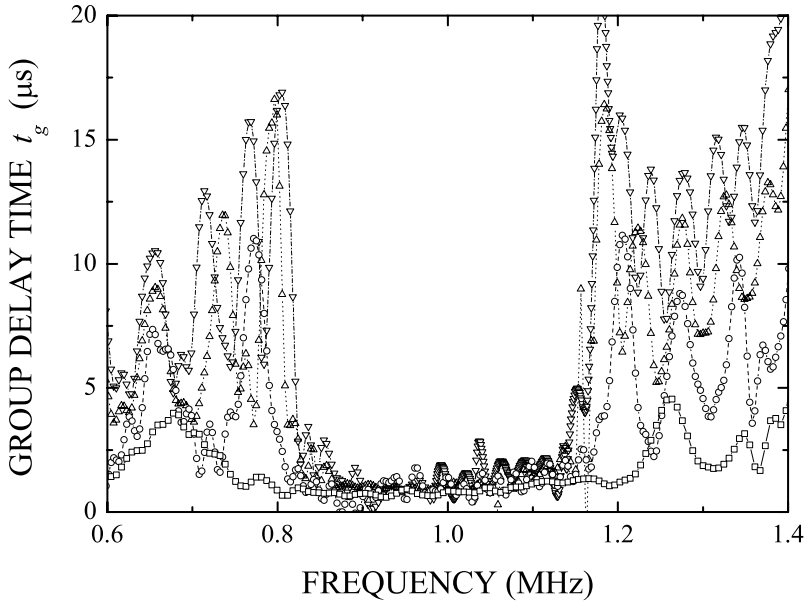

Figure 9. Measurements of the group delay time as a function of frequency for 4 phononic crystals containing 3, 6, 9 and 12 layers, corresponding to 1, 2, 3 and 4 complete unit cells along the [111] direction.

waves. This has the effect of increasing the transit time and hence reducing the group velocity. We can understand the effects of absorption on the group velocity by a 'two-modes' model, based on the simple approximation that pulse transport can be viewed as a dominant tunnelling process in parallel with a small propagating component. In this model, the group velocity can be estimated from the weighted average of the tunnelling time, $t_{\rm tun}$ and the propagation time $L/v_{\rm prop}$ [21]:

$$\bar{v}_g = \frac{L}{w_t t_{\rm tun} + w_p (L/v_{\rm prop})} \tag{4}$$

Note that $t_{\rm tun}$ and $v_{\rm prop}$, the group velocity of the propagating mode, are constant, independent of L. The weighting factors w_t and w_p are given by

$$w_t = \frac{c\ \exp[-L/(2l_{\rm tun})]}{c\ \exp[-L/(2l_{\rm tun})] + \sqrt{1-c^2}\ \exp[-L/(2l_{\rm prop})]} \tag{5}$$

$$w_p = \frac{\sqrt{1-c^2}\ \exp[-L/(2l_{\rm prop})]}{c\ \exp[-L/(2l_{\rm tun})] + \sqrt{1-c^2}\ \exp[-L/(2l_{\rm prop})]} \tag{6}$$

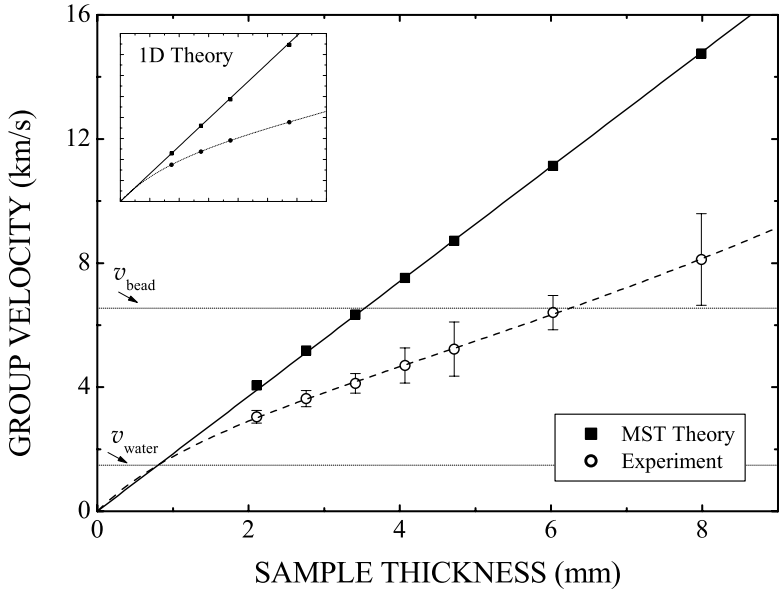

Figure 10. The group velocity as a function of sample thickness at 0.945 MHz. The horizontal dotted lines indicate the longitudinal velocities in water and tungsten carbide. The inset shows theoretical predictions in 1D for the group velocity with (solid circles) and without (solid squares) absorption. The dashed curves are fits of the two-modes model to the experimental data.

Here c is the coupling coefficient, and $l_{\rm tun}$ and $l_{\rm prop}$ are the extinction lengths of the tunnelling and propagating modes. Using the MST to calculate $t_{\rm tun} = 0.54$ μs and $l_{\rm tun} = 0.54$ mm, and taking $v_{\rm prop} = 1.5$ km/s (the group velocity in the water matrix), we fit Eq. (4) to the experimental data in Fig. 10 with $l_{\rm prop}$ and c as the only free parameters. We find that the empirical parameter describing the decay of the propagating mode is very similar to the tunnelling mode ($l_{\rm prop} = 0.47$ mm), so that the weighting factors are almost independent of thickness, and that $c = 0.96$, confirming that tunnelling is the dominant component. It can be seen from Fig. 10 that this simple phenomenological model gives an excellent fit to the data over the entire range of thicknesses. To check the validity of this approach, we have also calculated the group velocity for a 1D phononic crystal in which absorption can be included rigorously. As shown in the inset to Fig. 10, absorption reduces the group velocity in the gap; furthermore, we can explain the reduction in terms of the two-modes model by fitting Eq. (4) to the calculation with absorption, giving the dotted curve shown in the inset.

Thus, the two-modes model can successfully account for the effect of absorption in both cases. Note that the effects of absorption on wave transport in the gap are somewhat paradoxical, in the sense that absorption appears to modify tunnelling to produce a small-amplitude propagating component with a real wave vector, even though both absorption and tunnelling are themselves characterized by imaginary wave vectors.

It is important to recognize that the tunnelling time for ultrasonic waves in phononic crystals, both measured in these experiments and calculated from the MST theory, corresponds to the group delay time of a pulse. We have verified this directly by comparing the measured pulse delay time, defined as above by the time interval between the peaks of Gaussian input and transmitted pulses, and the group time $t_g = d\phi/d\omega$ determined by numerically differentiating the measured cumulative phase with respect to frequency. We find that the same values of $t_{\rm tun}$ are measured in both cases. Thus, some of the theoretical models of the tunnelling time [25, 26, 27, 28, 29, 30], such as the 'dwell time' or the Büttiker-Landauer 'semi-classical' time [25, 29], do not apply here. Our results for the tunnelling time in the middle of the gap are summarized in Fig. 11, where we plot the tunnelling time as a function of the thickness of the crystals. Both theory and experiment approach an asymptotic limit for the thicker samples that is independent of L. Moreover, even though the times are short by ultrasonic standards for samples up to 8 mm thick, being about 1 μs or less, they are long enough to be easy to measure compared with the tunnelling times in optical band gap experiments, which are about 9 orders of magnitude shorter [32, 31, 33]. This large difference in the magnitude of the tunnelling times is a consequence of the relation that we find between the tunnelling time and the gap width $\Delta\omega_{\rm gap}$, a relationship that also holds for the group delay of light and electrons (where for electrons $\Delta\omega_{\rm gap}$ corresponds to the barrier height): $t_{\rm tun} \sim 1/\Delta\omega_{\rm gap}$ in the middle of the gap.

The sample-thickness-independent tunnelling time observed in these and other experiments may be interpreted to imply that the group velocity can be greater than the speed of light for a sufficiently thick crystal (superluminal velocity). Does it violate causality? The answer is no. This superluminal phenomenon can be understood by a pulse reshaping process in which interference causes the later part of the pulse to be attenuated in such a way that the peak of the transmitted pulse shifts to an earlier time than that of the incident pulse. The energy transmitted at any time is much less than it would have been without the crystal in place; in fact for the values of the tunnelling time measured in our experiments, the thickness required for the group velocity to become superluminal is so great that the signal would be undetectably small (the relevant distance in everyday units

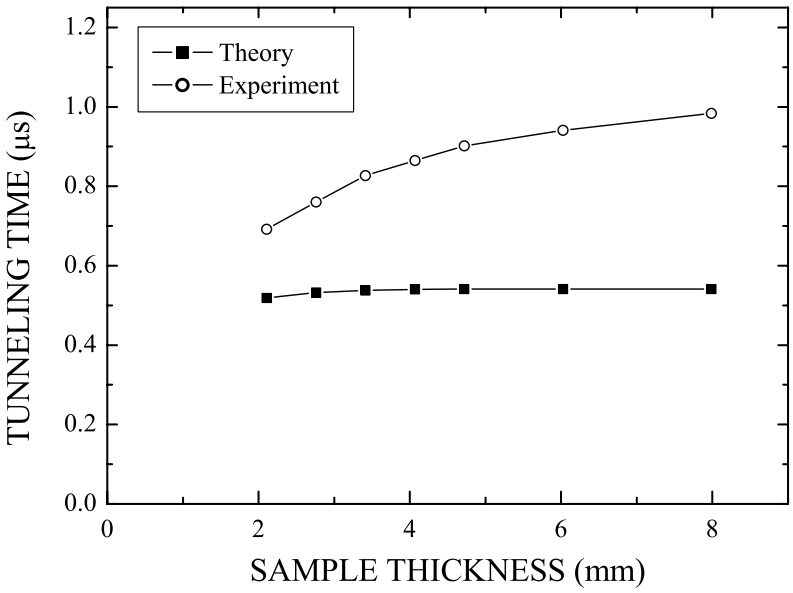

Figure 11. The tunnelling time as a function of sample thickness. For ultrasound tunnelling though a phononic crystal, the tunnelling time is equal to the group delay time.

amounts to the length of a football field!). Nonetheless, it may still be worth noting that the speed is 'supersonic' in the sense that it greatly exceeds the velocity of sound in water, which plays a role in these acoustic experiments that is analogous to the vacuum speed of light in optics experiments.

4. Near-field ultrasonic imaging of the wave field at the surface of phononic crystals

In this section, we give some examples of the wave field close to the surface of the phononic crystals consisting of tungsten carbide beads in water. We use an ultrasound field pattern imaging technique, in which a plane-wave pulse is incident on one face of the crystal and the transmitted field is measured near the opposite face using a small hydrophone detector. By studying these wave field patterns, a clear picture can be obtained of the behaviour of the displacement field and the distribution of energy in perfect crystals, as well as monitoring the effects of defects in imperfect crystals.

The wave amplitude just above the surface of a phononic crystal is not uniform, but varies in periodic patterns that reveal the underlying structure

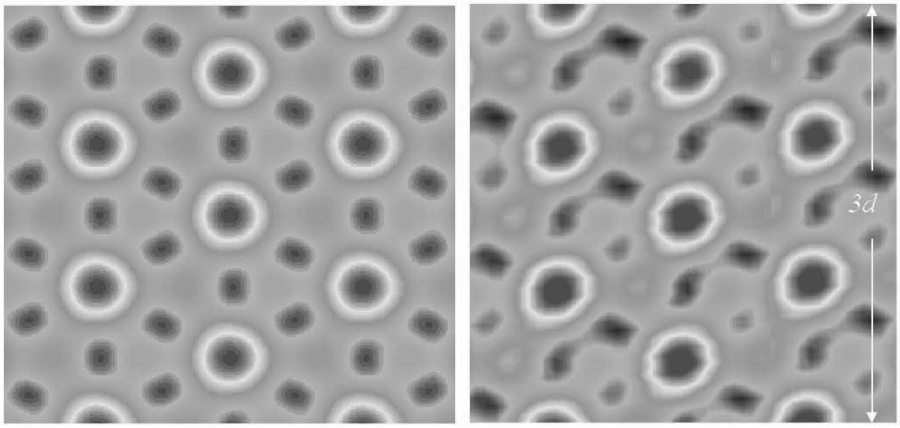

Figure 12. Theoretical (left) and experimental (right) near-field patterns for a 7-layer fcc crystal. The plane of the figure is perpendicular to the [111] direction. The height and width of the pictures are both equal to 3 bead diameters.

of the crystal. Figure 12 shows our theoretical and experimental near-field wave patterns 3 mm away from the crystal surface for a 7-layer crystal. These field patterns were measured and calculated using the MST at 2.5 MHz, well above the complete band gap. Despite the fact that the measured pattern is slightly tilted, due to a very small drift in the 2D scanner used to position the hydrophone, good agreement between the theory and experiment is observed. The pattern shows the 3-fold symmetry expected in a plane perpendicular to the [111] direction, and suggests that measurements of such periodic near-field diffraction patterns could provide a novel way of determining crystal structures. The pattern varies rapidly as the frequency is varied, while always preserving the underlying symmetry, giving additional information on the interference of the multiply scattered wave field inside the crystal. For example, peaks in the field pattern at 2.4 MHz were found to become valleys at 2.8 MHz, reflecting the very different spatial distribution of the wave energy that that results from only a modest change in the frequency ($\sim 15\%$).

Most crystals are usually not perfect, and imaging the location of defects can be important for understanding and controlling their physical properties. An example of a subsurface defect, whose presence could not detected

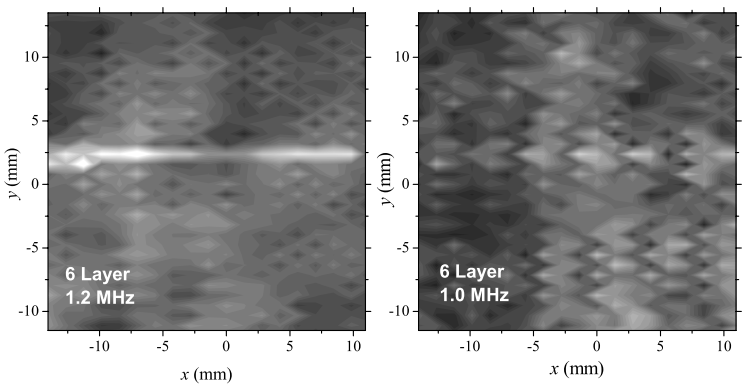

Figure 13. Image of a line defect in a 6-layer phononic crystal of tungsten carbide beads in water. The line defect shows up clearly as a bright streak in the image on the left, which was taken at a frequency just above the band gap, while it is barely visible in the image on the right, which was taken at a frequency in the gap.

by visual inspection of the crystal, is shown in Fig. 13. Here the presence of a line defect in a 6-layer phononic crystal shows up clearly when imaged at frequencies above the gap (left), but is barely detectable in the gap (right), illustrating the increased sensitivity to this type of defect in the pass band. As another example of imaging defects, we also studied a point defect (vacancy) in the middle of the top layer of the 7 layer phononic crystal. The measured wave field patterns both before and after removing one of the beads are shown in Fig. 14. It can be seen that the field pattern of the 'perfect' crystal has almost perfect periodicity (top right). For the crystal with the defect, the pattern changes around the vacancy, as can be see by comparing the magnified images before and after the defect was removed, (top and bottom left images in the figure). The field of view in the magnified images is approximately three bead diameters across, and the vacancy is located close to the centre. This figure shows that the effect of creating the vacancy is not to change the local symmetry of the field pattern, or to remove any of the features, but to substantially modify the amplitude of the field pattern in the vicinity of the defect. Rather surprisingly, the wave amplitude above the defect is smaller than for the perfect crystal, which is counterintuitive since one would naively imagine that removing a scatterer from the surface would enhance the field locally. To show this effect more clearly, the bottom right picture shows the difference between these two field patterns, providing a clearer indication of the location of the defect. These examples illustrate that studying such field patterns in

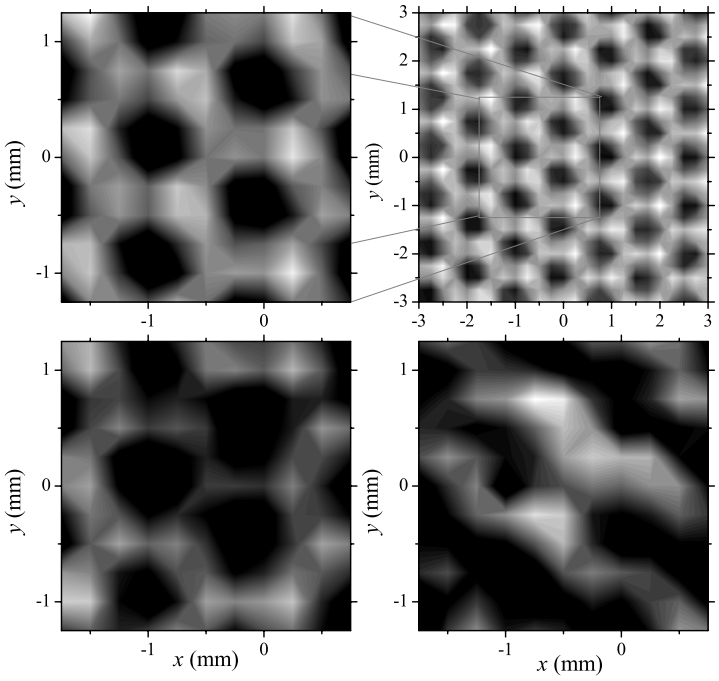

Figure 14. Observation of a point defect or vacancy created by removing one bead from the top layer of a 7-layer phononic crystal. The perfect lattice is shown in the top two images (the left picture being a magnified portion of the right picture). The lower left image shows the change in the field pattern as a result of removing the bead, while the difference (perfect crystal image minus the defect crystal image) is shown at the lower right. White corresponds to maximum amplitude and black to minimum amplitude.

phononic crystals may provide a novel opportunity for learning more about wave scattering and propagation inside periodic composite materials.

5. Focussing Ultrasound with Phononic Crystals

At frequencies outside the band gap, wave propagation is strongly influenced by the anisotropy of the dispersion relations, leading to interesting effects arising from the fact that the group velocity is no longer parallel to the wave vector. In atomic crystals, analogous effects, known as phonon focussing, have been extensively studied [34], but experiments are limited to the long wavelength regime where $\lambda \gg a$. To investigate phonon focussing at frequencies above the first band gap in the tungsten carbide/water phononic crystal, we replaced the quasi plane-wave source used in the ex-

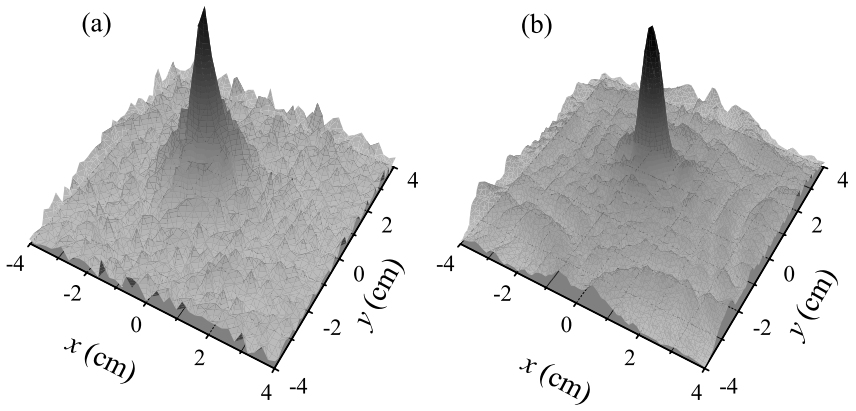

Figure 15. The spatial variation of the wave amplitude in a plane parallel to the surface of a tungsten-carbide/water phononic crystal when an incident point-like source is placed on the opposite side of the crystal. The frequency is 1.57 MHz. Instead of the diverging beam seen without the crystal in place, a tightly focused spot is observed. Fig. (a) shows the experimental data and (b) shows the theoretical prediction using a Fourier imaging technique, in which wave propagation through the crystal is described by the dispersion surface calculated using the MST.

periments described above with a small-diameter disk-shaped transducer, which acts as a good approximation to a point source. The source transducer was placed close to the sample surface (3 mm, or approximately 2 wavelengths, away). The field pattern on the far side of the crystal and substrate was measured by scanning a small hydrophone, which had a diameter much less than the ultrasonic wavelength, in a plane parallel to the crystal surface. The experiments were performed with pulses. By taking FFTs of each pulse, the amplitude of the transmitted field at any frequency in the bandwidth of the pulse could then be measured as a function of position in the detecting plane.

As the frequency is varied, the detected field pattern varies widely, a result of the rapid changes in the anisotropy of the dispersion relations with frequency that take place in the higher pass bands (see Fig. 2 and Refs. [35]. One example of the measured field patterns for a 12-layer tungsten-

carbide/water crystal is shown in Fig. 15(a); this pattern was measured at 1.57 MHz, which corresponds to a reduced frequency of 1.2 near the bottom of the third pass band along the ΓL direction (Fig. 2(b)). The figure shows that the diverging beam from the source transducer, which has a FWHM in the detection plane of 65 mm (more than three quarters of the width of the region imaged in the figure), is sharply focussed to a tight spot with a FWHM of only 5 mm. Thus, it is clear from this example that a phononic crystal with flat parallel planar faces can be used to focus ultrasound. One remarkable feature of these data is that such a sharp focal spot is observed in a plane quite far from the crystal; the distance from the crystal face to the detection plane is approximately 130 wavelengths, while the distance from the source to the crystal is only 2 wavelengths.

The origin of the focussing effect can be understood from the dispersion (or slowness) surface, which, for constant frequency, represents the variation in the magnitude of the wave vector with direction. To interpret our data, we calculated the dispersion surface using the MST, solving for the magnitudes of the wave vectors along different wave vector directions at a particular frequency, in the same way as the band structure is calculated for different eigenfrequencies along particular wave vector directions. To represent forward propagation through the crystal at frequencies near 1.6 MHz, the dispersion surface calculated in the reduced Brillouin zone was translated to the extended zone, the correct translation being from $\vec{k}$ to $\vec{k}-2\vec{G}_{111}$ in this case. Figure 16 shows a 3D plot of the dispersion surface for wave vectors near the ΓL (or [111]) direction. It can be seen that the dispersion surface has a pronounced minimum for $\vec{k}$ parallel to the [111] direction. Consequently, the normal to the dispersion surface, which represents the direction of the group velocity and hence the direction in which energy is transported inside the crystal, points back towards the [111] direction as the direction of the wave vector moves away from the [111] direction. This large anisotropy results in 'negative refraction' without a negative refractive index; this occurs since the net wave transport inside the crystal follows the directions of the group velocity, which points in directions that correspond to negative angles of refraction. However, it is important to remember that this is not a refraction phenomenon in the usual sense, since its origin is the direction of the group velocity and not the wave vector. The dip in the dispersion surface shown in Fig. 16 is quite deep, resulting in large effective 'negative refraction'; as a result, it is possible for the waves passing through the crystal to form a tight focal spot quite far away from the crystal even when the crystal is only 12 layers thick.

To interpret our data quantitatively, we calculated the field pattern corresponding to the data shown in Fig. 15(a) using a Fourier imaging technique. After the input beam is Fourier transformed spatially into plane

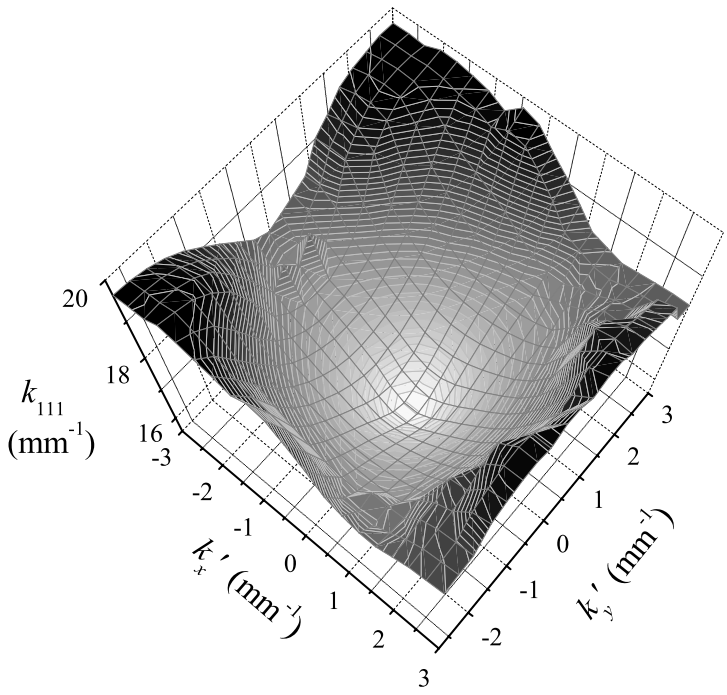

Figure 16. A 3D plot of the dispersion surface for wave vectors near the ΓL ([111]) direction. The dispersion surface is shown in the extended zone scheme, which also corresponds to part of the periodic zone scheme representation centred at $2G_{\Gamma L}$. The directions of k_x' and k_y' are parallel to the LK and LW directions, respectively. The frequency used in these calculations corresponds to the same frequency relative to the band edge as in the experimental data shown in Fig. 15.

waves, each plane wave is allowed to propagate through the crystal according to the wave vectors determined by its dispersion surface, accounting correctly for refraction at the front and back interfaces (i.e. the components of the wave vector parallel to the surface remain the same inside and outside the crystal). The field pattern in the detecting plane is then reconstructed by taking an inverse Fourier transform back into real space, giving the results shown in Fig. 15(b). Excellent agreement with experiment is seen, confirming that this model correctly incorporates the essential physics of this wave focussing phenomenon.

Ultrasonic pulse propagation in phononic crystals is making an important contribution to understanding wave transport in ordered structures. Because the wave field is measured directly in ultrasonic experiments, a complete picture of wave propagation is accessible, allowing the transmission coefficient, the dispersion relations and the dynamics of the wave fields to be investigated. In this paper, we have concentrated on two different types of wave phenomena in 3D phononic crystals: ultrasound tunnelling and focussing by 'negative refraction'. Some examples of near-field imaging experiments have also been presented.

We have summarized recent progress in demonstrating the tunnelling of ultrasonic wave pulses through a complete band gap, showing that remarkably large values of the group velocity can be measured, as the group velocity is proportional to sample thickness. The classic signature of tunnelling, that the tunnelling time is independent of sample thickness for thick samples, has been demonstrated, and its magnitude found to be equal to the reciprocal of the gap width in the middle of the gap. The experimental results have been interpreted using the Multiple Scattering Theory, which was found to give good overall agreement. The counterintuitive effects of absorption on the tunnelling dynamics were also investigated and interpreted using a simple 'two-modes' model; this model shows that the effect of absorption on evanescent waves in band gap materials is to modify their character by introducing a small propagating component.

The concave character of the dispersion surfaces in phononic crystals (as viewed looking back towards the origin) has been shown to lead to the focusing of ultrasonic waves from a diverging source in the absence of the usual curved surfaces employed in traditional lenses. Again the MST theory provides an excellent basis for understanding the experimental results, and gives predictions that are in good agreement with experiment. We are currently examining the behaviour at other frequencies and extending this work to solid 3D phononic crystals, which are easier to handle and more useful for practical applications.

6. Acknowledgements

Support from the Natural Sciences and Engineering Research Council of Canada and the RGC (HKUST6143/00P) of Hong Kong is gratefully acknowledged.

7. References

References

1. Author to whom correspondence should be addressed. Email: jhpage@cc.umanitoba.ca Website: www.physics.umanitoba.ca/∼jhpage.
2. Current address: Energenius Centre for Advanced Nanotechnology, University of Toronto, 170 College St. Toronto, Ontario, Canada, M5S 3E3. Suxia Yang was also a student at the Hong Kong University of Science and Technology while this research was performed.
3. Current address: Dept. of Physics, University of Toronto, 60 St. George St., Toronto, Ontario Canada M5S 1A7.
4. M. Sigalas and E. N. Economou, *Solid State Communications* **86**, 141 (1993).
5. E. N. Economou and M. Sigalas, *J. Acoust. Soc. Am.* **95**, 1734 (1994).
6. M. S. Kushwaha, P. Halevi, and G. Martinez, *Phys. Rev. B* **49**, 2313 (1994).
7. R. Mártinez-Sala, J. Sancho, J. V. Sánchez, J. Linres, and F. Mesegure, *Nature* **378**, 241 (1995).
8. F. R. Montero de Espinosa, E. Jiménez, and M. Torres, *Phys. Rev. Lett.* **80**, 1208 (1998).
9. J. O. Vasseur, P. A. Deymier, G. Frantziskonis, G. Hong, B. Dijafari-Rouhani, and L. Dobrzynski, *J.Phys.: Condens. Matter* **10**, 6051 (1998).
10. M. Torres, F. R. Montero de Espinosa, D. García-Pablos, and N. Garcí́a, *Phys. Rev. Lett.* **82**, 3054 (1999).
11. M. Kafesaki and E. N. Economou, *Phys. Rev. B* **60**, 11993 (1999).
12. I. E. Psarobas, N. Stefanou, and A. Modinos, *Phys. Rev. B* **62**, 278 (2000).
13. Z. Liu, C. T. Chan, P. Sheng, A. L. Goertzen, and J. H. Page, *Phys. Rev. B* **62**, 2446 (2000).
14. Z. Liu, X. Zhang, Y. Mao, Y. Y. Zhu, Z. Yang, C. T. Chan, and P. Sheng, *Science* **289**, 1734 (2000).
15. J. H. Page, A. L. Goertzen, S. Yang, Z. Liu, C. T. Chan, and P. Sheng, in *Photonic Crystals and Light Localization in the 21st Century*, edited by C. M. Soukoulis (Kluwer Academic Publishers, Amsterdam, 2001), p. 59.
16. M. Torres, F. R. Montero de Espinosa, and J. L. Aragón, *Phys. Rev. Lett.* **86**, 4282 (2001).
17. Suxia Yang, J. H. Page, Zhengyou Liu, M. L. Cowan, C. T. Chan, and Ping Sheng, *Phys. Rev. Lett.* **88**, 104301 (2002).
18. E. Yablonovitch, *Phys. Rev. Lett.* **58**, 2059 (1987).
19. S. John, *Phys. Rev. Lett.* **58**, 2486 (1987).
20. *Photonic Crystals and Light Localization in the 21st Century*, edited by C. M. Soukoulis (Kluwer Academic Publishers, Amsterdam, 2001)
21. Suxia Yang, *Ph.D Thesis*, (The Hong Kong University of Science and Techology, 2002)
22. As is well known, the first Brillouin zone for the fcc structure is closer to a spherical shape than for hcp, and this facilitates the formation of a complete gap.
23. For a review of tunneling times with particular reference to photon tunnelling, see R. Y. Chiao and A. M. Steinberg, in *Progress in Optics*, edited by E. Wolf, Vol. 37, (Elsevier, Amsterdam, 1997), p. 347.
24. A rigorous first-principles calculation of ultrasonic absorption in the crystal remains a challenging problem. Mechanisms involving interfacial effects are difficult to incorporate in the MST model because of problems with an ill-conditioned matrix when the effects of viscosity in the liquid are included.
25. M. Büttiker and R. Landauer, *Phys. Rev. Lett.* **49**, 1739 (1982).
26. E.H. Hauge, J.P. Falck and T.A. Fjeldly, *Phys. Rev. B* **36**, 4203 (1987).
27. E.H. Hauge and J.A.Støvneng, *Rev. Mod. Phys.* **61**, 917 (1989).
28. R. Landauer, *Nature* **341**, 567 (1989).

29. M. Büttiker, in *Electronic Properties of Multilayers and Low-Dimensional Semiconductor Structures*, edited by J. M. Chamberlain, *et al.* (Plenum Press, New York, 1990) p. 297
30. R. Y. Chiao and A. M. Steinberg, in *Progress in Optics*, edited by E. Wolf, Vol. 37, (Elsevier, Amsterdam, 1997), p. 347.
31. A. M. Steinberg, P. G. Kwist, and R. Y. Chiao, *Phys. Rev. Lett.* **71**, 708 (1993).
32. C. Spielmann, R. Szipocs, A. Stingl, and F. Krausz, *Phys. Rev. Lett.* **73**, 2308 (1994).
33. M. Mojahedi, E. Schamiloglu, F. Hegeler, and K. J. Malloy, *Phys. Rev. E* **62**, 5758 (2000).
34. J. P. Wolfe, *Imaging Phonons: Acoustic Wave Propagation in Solids* (Cambridge University Press, Cambridge, 1998).
35. H. Kosaka, T. Kawashima, A. Tomita, M. Notomi, T. Tamamura, T. Sato and S. Kawakami, *Phys. Rev. B* **58**, 10096 (1998); *Appl., Phys. Lett.* **74**, 1212 (1999); *Appl., Phys. Lett.* **74**, 1370 (1999).